ABSTRACT

INELASTIC PROTON SCATTERING AT 40 MeV
FROM THE EVEN NICKEL ISOTOPES

By

Kenneth M. Thompson

A study of inelastic scattering from the even nickel isotopes has been done using 40 MeV protons from the Michigan State University sector focused cyclotron. Angular distributions from about 15° to 90° were obtained for each nucleus in 5° steps using Ge(Li) charged particle detectors. The best energy resolution achieved was 45 keV. All of the resulting angular distributions are presented in both a tabular and a graphical form.

A high precision goniometer was designed and constructed to facilitate the use of Ge(Li) detectors. The details of the construction of this apparatus are given. Also described in detail are the procedures used in the calibrations of the remotely operated detector support and target positioning mechanisms.

The experimental angular distributions for all of the observed states were compared with calculated distributions using a collective model distorted wave theory. From these comparisons values for the nuclear deformation parameters,

β_L, were obtained. The resulting nuclear deformations, $\beta_L R_o$, were used to calculate the vibrational model parameters and the reduced transition probabilities. The deformations were also compared to results from other experiments. The fractional depletion of an energy weighted sum rule and a sum rule based on the shell-model were also calculated for each state. The dependence of the reduced transition probabilities and sum rule limits on the model used for the nuclear charge density was also examined. The results of these calculations for a uniform charge density with r_o = 1.20F and r_o = 1.31F are given along with those for a Fermi distribution with r_o = 1.10F and a = 0.566F. These are tabulated for all of the observed states.

Comparisons of the calculated quantities were made with results of experimental studies of electromagnetic transitions in the nickel isotopes. There were also comparisons made with the results of calculations using strongly admixed spherical shell model configurations done by N. Auerbach and a modified Tamm-Dancoff approximation done by Ram Raj et al.

INELASTIC PROTON SCATTERING AT 40 MeV FROM THE EVEN NICKEL ISOTOPES

By

Kenneth M. Thompson

A THESIS

Submitted to
Michigan State University
in partial fulfillment of the requirements
for the degree of

DOCTOR OF PHILOSOPHY

Department of Physics

1969

ACKNOWLEDGMENTS

I am greatly indebted to Dr. Charles Gruhn for his guidance, encouragement, and assistance throughout my graduate work and particularly during the work for this thesis.

I am also grateful to Dr. Barry Preedom for his assistance in the understanding and the implimentation of the techniques of the distorted wave analysis needed for this work. I also acknowledge the many helpful discussions with the professional staff of the Michigan State University Cyclotron Laboratory.

Thanks go to many who aided in the design and construction of the goniometer used in this experiment--to Dr. William Johnson, Robert deForest and the staff of the electronics shop for their help in the design and constuction of the electrical and electronics systems; to Norval Mercer, the staff of the mechanical shop, Gunther Stork, David Rozof, and the members of the technical staff for their help in the design, construction, and assembly of the mechanical systems; and to Andrew Kaye for his help in procurring the necessary raw materials.

I am also grateful to my fellow graduate students for their helpful discussions throughout this work but

especially to Carl Maggiore, Tom Kuo, Larry Samuelson, and Bill Seidler for their assistance during the data acquisition for this experiment. Also the aid of the computer personnel is acknowledged as is their provision of the software which established a time sharing computer system which greatly facilitated the analysis of the data.

I also acknowledge the financial support of the research program at MSU provided by the National Science Foundation and the personal support from the NSF during the work for this thesis.

A very special thanks go to Mom and Dad for their support and encouragement during my graduate studies.

TABLE OF CONTENTS

		Page
ACKNOWLEDGMENTS		ii
LIST OF TABLES.		vii
LIST OF FIGURES		ix
Chapter		
I.	INTRODUCTION.	1
II.	HIGH PRECISION GONIOMETER	5
2.1	Design Features	5
2.1.a	The Ge(Li) Detector Package.	7
2.1.b	List of Included Features	10
2.2	Goniometer Construction and Operation.	12
2.2.a	Goniometer Drive	13
2.2.b	Local Electrical System	19
2.2.c	Remote Control Panel	19
2.3	Calibration of the Goniometer	23
2.3.a	Main Arm Angle Calibration	24
2.3.b	Target Angle.	39
2.3.c	Target Height	42
2.3.d	Concentricity Checks	44
2.4	Installation.	45
III.	EXPERIMENTAL PROCEDURES	51
3.1	Cyclotron and Beam Transport System.	51
3.1.a	Cyclotron.	51
3.1.b	Beam Transport System.	51
3.1.c	Alignment of the Beam into the Target Chamber	53
3.1.d	Faraday Cup and Current Integrator	54
3.2	Set up of the Goniometer.	56
3.2.a	Target Chamber	56
3.2.b	Targets	56
3.2.c	Detectors.	56
3.3	Electronics	59
3.4	Data Acquisition	63

Chapter		Page
IV.	DATA ANALYSIS	69
	4.1 Experimental Analysis.	69
	4.1.a Computer Programs Used	70
	4.1.a.1 Peakstrip	70
	4.1.a.2 Reltomon	70
	4.1.a.3 Foiltarcal.	71
	4.1.a.4 Sigtote.	72
	4.1.b Lab Angle Calibration.	73
	4.1.c Elastic Cross Sections	75
	4.1.d Normalization of the Data to Obtain Absolute Cross Sections.	76
	4.1.d.1 Dead Time	76
	4.1.d.2 Ratios of the Monitor Counts to the Integrated Current.	76
	4.1.d.3 Method of Normalization	77
	4.1.d.4 Corrections	78
	4.1.d.5 Final Results.	80
	4.1.e Inelastic Angular Distributions	81
	4.1.f Excitation Energies	82
	4.2 Theroetical Analysis	88
	4.2.a DWBA Theory	88
	4.2.b Vibrational Model Parameters and Reduced Transition Probabilities	95
	4.2.c Sum Rules.	98
	4.2.d Optical Model Parameters.	99
	4.2.e DWBA Calculations	102
	4.2.f Extraction of Deformation Parameters, β_L	104
V.	DISCUSSION OF THE RESULTS	117
	5.1 Comparisons with Other Experiments	120
	5.2 Comparison with Theory	126
	5.3 Conclusions	128
APPENDICES		133
I.	Details of the Construction and Operation of the Goniometer	136
II.	Calculations of the Angles in Reference I Used for the Main Arm Calibrations.	216
III.	Compounding of the Errors in the Points for the Main Arm Reference Angles	218

APPENDICES

Page

IV. Experimental Data 227

IV.1 Tabulated Angular Distributions
IV.2 Plotted Angular Distributions
IV.3 Tabulated Nuclear Deformations
IV.4 Tabulation of Quantities Calculated from the Nuclear Deformation in IV.3

REFERENCES 284

LIST OF TABLES

Table		Page
2.1	The reference I angles and estimated standard errors.	31
2.2	Summary of the results of the calibration of the main arm.	38
2.3	Summary of the results of the calibration of the target angle	41
2.4	Summary of the results of the calibration of the target height	44
2.5	Summary of the results of the concentricity checks.	45
3.1	The self-supporting foil targets used . . .	57
4.1	Excitation energies for ^{58}Ni	84
4.2	Excitation energies for ^{60}Ni	85
4.3	Excitation energies for ^{62}Ni	86
4.4	Excitation energies for ^{64}Ni	87
4.5	Average optical potential parameters used. .	100
4.6	Optical potential strength parameters used .	102
4.7	J^{π} assignments for states in ^{58}Ni and the excitation energies and L-values used in this experiment.	105
4.8	J^{π} assignments for states in ^{60}Ni and the excitation energies and L-values used in this experiment.	106
4.9	J^{π} assignments for states in ^{62}NI and the excitation energies and L-values used in this experiment.	107
4.10	J^{π} assignments for states in ^{64}Ni and the excitation energies and L-values used in this experiment.	108

Table		Page
4.11	Estimated upper limites for the δ_L for the second 2+ states	116
5.1	Tentative L assignments.	119
5.2	Nuclear deformations for ^{58}Ni and comparison with experiments representative of other reactions.	121
5.3	Nuclear deformations for ^{60}Ni and comparison with experiments representative of other reactions.	122
5.4	Nuclear deformations for ^{62}Ni and comparison with experiments representative of other reactions.	123
5.5	Nuclear deformations for ^{64}Ni and comparison with experiments representative of other reactions.	123
5.6	Comparisons of reduced transition probabilities, B(EL; 0→L), in units of F^{2L}. . . .	124
5.7	Experimental surface tension parameters, C_L(MeV)	125
5.8	Experimental mass transport parameters, $D_L/\hbar^2$, in units of (MeV^{-1})	126
5.9	Experimental and theoretical results for B(E2)'s in the nickel isotopes.	127
5.10	Experimental and theoretical results for B(E2)'s for the nickel isotopes. The effective charge assumed in the theoretical calculations was 1.35e	129
III.1	Estimated standard errors for the primary angles in reference I for the main arm due to errors in the linear measurements .	223
III.2	Estimated standard errors for the primary points in reference I due to the error in the central, 90° angle	225
III.3	Total estimated standard errors in the primary points in reference I	225
III.4	Total estimated standard errors in the secondary points in reference I	226

LIST OF FIGURES

Figure		Page
2.1	Vertical cryostat Ge(Li) detector package .	8
2.2	Goniometer drive unit	14
2.3	Local control box	20
2.4	Remote control panel	21
2.5	Floor plan of the geometry for the primary points in reference I	26
2.6	Floor plan of the geometry used in the 90° transfer of the primary angles of reference I.	30
3.1	Experimental area of the Michigan State University Cyclotron Laboratory	52
3.2	Block diagram of the electronics used with the Ge(Li) detectors.	60
3.3	Block diagram of the electronics used with the monitor counter	62
3.4	$^{58}Ni(p,p')^{58}Ni$ spectrum at $\theta_{LAB} = 29.4°$ for Ep = 40 MeV.	65
3.5	$^{60}Ni(p,p')^{60}Ni$ spectrum at $\theta_{LAB} = 57.8°$ for Ep = 40 MeV.	66
3.6	$^{62}Ni(p,p')^{62}Ni$ spectrum at $\theta_{LAB} = 47.8°$ for Ep = 40 MeV.	67
3.7	$^{64}Ni(p,p')^{64}Ni$ spectrum at $\theta_{LAB} = 47.8°$ for Ep = 40 MeV.	68
4.1	Comparisons of the experimental, elastic scattering results and the theoretical calculations using the optical potential parameters given in Tables 4.5 and 4.6 .	103

Figure		Page
4.2	Comparisons of the experimental inelastic scattering results and the theoretical DWBA calculations for states in ^{58}Ni with known J^{π} assignments.	110
4.3	Comparisons of the experimental inelastic scattering results and the theoretical DWBA calculations for states in ^{58}Ni with known J^{π} assignments.	111
4.4	Comparisons of the experimental inelastic scattering results and the theoretical DWBA calculations for states in ^{60}Ni with known J^{π} assignments.	112
4.5	Comparisons of the experimental inelastic scattering results and the theoretical DWBA calculations for states in ^{62}Ni with known J^{π} assignments.	113
4.6	Comparisons of the experimental inelastic scattering results and the theoretical DWBA calculations for states in ^{64}Ni with known J^{π} assignments.	114
I.1	Schematic of the structure of the main arm used to calculate the location of the point (A) at which the brace meets the main arm. .	139
I.2	Results of the calculations and measurements of the vertical deflections in the main arm under a load of 100 lbs.	141
I.3	Section view of the 4:1 gear train for the main arm drive.	147
I.4	Plot of the speed factor, X_s, versus angular velocity, RPM	157
I.5	Section view of central column	173
I.6	Section view of the target chamber and sliding vacuum seal.	180
I.7	Remote control panel	195
II.1	Schematic of the geometry used to calculate the angular position of the primary points of reference I used in the calibrations of the main arm	217

CHAPTER I

INTRODUCTION

In recent years there have been many studies done in the $2p_{3/2}$, $1f_{5/2}$, $2p_{1/2}$ region of the periodic table. Of particular interest in this thesis is the work that has been done on the stable even nickel isotopes ^{58}Ni, ^{60}Ni, ^{62}Ni, and ^{64}Ni. Fricke et al. (Fr 67b)*, for example, have used elastically scattered protons and their measured polarization to establish the optical model potentials for ^{58}Ni and ^{60}Ni at 40 MeV. Fricke et al. have also studied the inelastic scattering and the inelastic asymmetries of 40 MeV protons from the highly excited first 2^+ and 3^- states in ^{58}Ni and ^{60}Ni (Fr 67c). There have also been a number of other studies involving these targets: for example (α, α') on ^{58}Ni and ^{60}Ni (Ja 67) (In 68), (d,d') on ^{58}Ni, ^{60}Ni, ^{62}Ni (Jo 69), and (e,e') on ^{58}Ni, ^{60}Ni (Cr 61) and on ^{58}Ni, ^{60}Ni, ^{62}Ni (Du 67). In most of these experiments the emphasis was placed on the strongly excited states.

In addition to these experiments theoretical calculations of the excited levels and reduced transition

*The references are specified by the first two letters of the primary author's surname followed by the year of publication. These are listed alphabetically at the end of the thesis.

probabilities have been made for these isotopes. N. Auerbach has, for example, described the nickel isotopes in terms of strongly admixed spherical shell-model neutron configurations (Au 67). Raj et al. have also done calculations for the even nickel isotopes using a modified Tamm-Dancoff approximation (Ra 67).

As pointed out by Glendenning and Veneroni (Gl 66) the proton is a useful probe of the microscopic structure of the nucleus. They calculate the (p,p') angular distributions of the low lying levels of the nickel isotopes using a microscopic description of the excitations. Comparison of results of the present work with these calculations are not given in this thesis, but these comparisons are expected to be made in the near future.

The nature of these experiments and theoretical calculations revealed the need to do a systematic study. The study which was done for this thesis, therefore, involved the examination of inelastically scattered, 40 MeV protons from the even nickel isotopes. For such a study to render information to test the microscopic interpretations, angular distributions were needed for the weakly excited states as well as for the strong, collective states.

In order to obtain these distributions a detection system was needed which had good resolution and which would minimize the background contributions.

A Ge(Li) charged particle detector was selected for this experiment. In order to facilitate the use of this detector system, a "spider" geometry scattering rig was designed and constructed. The details of the design and construction of this goniometer, i.e., angular measuring device, are given in Chapter II and Appendix I.

The collective model distorted wave theory (Ba 62) (Sa 64) was used in the analysis of the angular distributions obtained in this experiment. This type of analysis has developed into a widely accepted method and therefore provides results which can be readily compared or reproduced if necessary. The optical model parameters used in the calculations were obtained from Fricke et al. (Fr 67b). The analysis of the present data yielded deformation parameters, β_L, for the observed states.

There is evidence that the low lying excited levels of the nickel isotopes are vibrational in character (La 64) (Bo 67a). For this reason the vibrational parameters associated with the observed states were calculated.

Recent studies of electron scattering from the nickel isotopes (Du 67) (Cr 61) yielded values for the reduced transition probabilities for various states; therefore, the B(EL)'s were also calculated for the present experiment to allow comparisons with those earlier experiments as well as with several theoretical estimates.

Using the comparisons between the results of this experiment and other experimental and theoretical studies it was possible to draw some conclusions concerning the extraction of model dependent parameters from the experimental data and the consistancy of several theoretical approaches.

CHAPTER II

HIGH PRECISION GONIOMETER

Before the data for this thesis was acquired, the instrumentation needed for obtaining angular distributions of charged particles using Ge(Li) detectors was designed and built. The form of construction used in the final system is a "spider" geometry similar to that used by others (He68a) (Ca67). This consists of detector positioning elements outside of a central vacuum chamber with the detectors viewing the targets through a sliding vacuum seal. The alternative vacuum pot configuration, in contrast, consists of a vacuum chamber containing the detection instruments and targets. This vacuum pot design, however, was less compatible with our experimental requirements. Since the fundamental purpose of this instrument is to measure the angular positions of detectors, it is called a goniometer.

2.1 Design Features

This device was built to facilitate charged particle, nuclear reaction studies in the energy range of 20-75 MeV. In particular the design was guided by the experimental requirements of inelastic proton scattering and ^{3}He

induced reactions. Among the proposed experiments, there were many which needed to use Ge(Li) charged particle detectors because of their energy resolving capabilities. Such detectors have been successfully fabricated at Michigan State University Cyclotron Laboratory (MSUCL) by a group supervised by C. R. Gruhn (Gr 68). They have been shown to be capable of giving energy resolution of 22 keV FWHM for 40 MeV protons (Gr 68a). Several types of packages were tried by this group for maintaining these detectors at liquid nitrogen (LN_2) temperatures in a vacuum environment. A package similar to the vertical cryostat design of Chasman (Ch 65) was found to be most convenient, and, therefore, the final design of the goniometer was made to be compatible with such a package.

The final configuration of this device is the result of compromising on several points. The results of a number of experiments representative of a variety of reactions were examined. The largest fractional change in the differential cross sections corresponding to an angular variation of 0.01° was estimated in each case. A maximum fractional change of 2% was defined as being acceptable. This required an angular precision of at least 0.02° in the majority of cases examined.

In order to obtain high angular precision as well as to allow for flexibility in the use of this device, the final design incorporated a 4 foot radius detector support called the main arm. This arm can be remotely positioned

with an accuracy of ±0.02° relative to a reference direction. Implementing a support capable of holding a vertical cryostat, detector package at this radius inside a vacuum pot scattering chamber would necessitate a very large vacuum system. The chamber would be prohibitive in cost, and the necessary evacuation times along with the difficulty of reaching the interior points would make this approach unacceptable. The spider geometry, on the other hand, avoids these problems since the detector positioning elements are located outside of a small, central, target vacuum chamber.

2.1.a The Ge(Li) Detector Package--Figure 2.1

The Ge(Li) charged particle detector configurations which have been used at MSUCL have been discussed elsewhere (Gr 68)(Gr 68a). The detector package which was found to be most convenient to use is a vertical cryostat design. The final goniometer design facilitates the use of this type of package. The final configuration does not, however, prevent the use of other choices of detectors or detector packages.

The Ge(Li) detector needs to be kept constantly in a vacuum and at temperatures near the boiling point of LN_2, 77°K. This vertical cryostat design contains an isolated, copper cold finger which is put into LN_2 and is in thermal contact with the detector. The vacuum is maintained inside

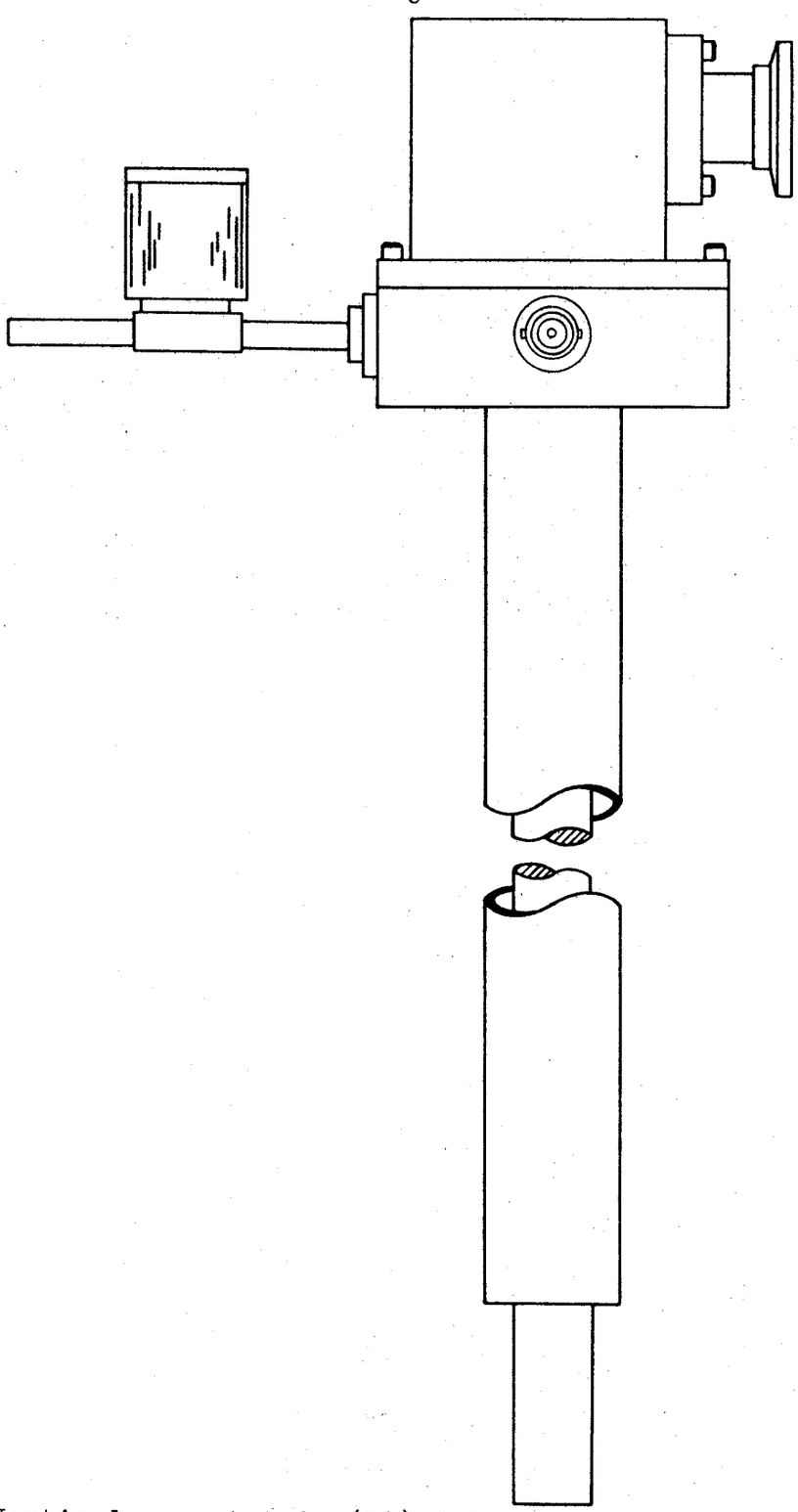

2.1 Vertical cryostat Ge (Li) detector package.

the enclosure by a cryopumping agent. The portion of the package containing the cold finger and cryopump can be inserted into the neck of a standard, 25 liter, LN_2 dewar permitting the storage of the system for up to 2 weeks without refilling.

The detector mount connected to the cold finger contains the collimator which defines the solid angle of the detector system. The package cap which encloses this mount contains an entrance port for the scattered particles. The exact details of this port and of the coupling used between this package and the target chamber depend on the requirements of the experiment. Several possible configurations are described here.

The package itself may contain a thin foil window. This window must be opaque and be able to sustain atmospheric pressures. It must, however, produce a minimum energy straggling contribution in the scattered particles. Windows that have proven successful in covering holes up to 3/8 inch in diameter are 1/10 mil Havar* and 1/4 mil, aluminized mylar. The staggling contributions have been calculated for 40 MeV protons to be about 9 keV and 3 keV respectively. The calculations use a computer program, TARGET, by J. J. Kolata. This program incorporates calculations of the Vavilov distribution of the energy of the transmitted particles. These windows have been glued to the aluminum cap using Eastman 910 adhesive.

*Hamilton Watch Company, Lancaster, Pennsylvania.

The package can be coupled to the foil window of the target chamber (see Appendix I) by using an evacuated tube with a thin foil window on each end. One of these additional windows can be eliminated by coupling the tube directly to the cap through an O-ring seal. A second window can be eliminated by permanently coupling the tube to the cap and removing the window on the cap itself.

The KF-20 Leybold vacuum fitting shown in Figure 2.1 is attached to the cap through an O-ring seal. This fitting allows the convenient implementation of the second arrangement described above. It also provides a means of coupling the detector to the target chamber through a pipe attached to the sliding seal. The window on the cap can also be eliminated by connecting a ball valve, for example, to this fitting. This allows the detector to view the target through the sliding seal in a windowless geometry providing the ultimate conditions for high resolution experiments.

2.1.b. List of Included Features

In addition to the aspects described above there are additional features included in this goniometer which add to its versatility and convenience. The following list enumerates these features as well as those presented above and those of general interest. These are described in detail in section 2.2 and Appendix I.

1. An adjustable stand which permits adjustment of both the vertical and horizontal position, and the levelness.
2. A remotely movable 4-foot radius detector support, the main arm, capable of holding a vertical cryostat for Ge(Li) detectors and the associated LN_2 dewar, or a maximum of 100 lbs at 4 feet.
3. A precision of ±0.02° in positioning the main arm.
4. A manually positioned secondary arm that can be positioned to ±0.1° and can support a maximum of 50 lbs at 2 feet.
5. A central, target vacuum chamber compatible with a sliding vacuum seal or with a thin foil window.
6. A target transfer and hold lock.
7. A target height positioning system with a precision of ±1 mil.
8. An automatic target selection system for three targets.
9. A vernier dial readout for the main arm position capable of being read through a television system to 0.005°.
10. A target rotating system with a precision of ±0.3°.
11. A local control of all functions.

12. Independent, remote digital readouts for the main arm, target angle, and target height positions.
13. A remote, graphic readout system which indicates the relative angular positions of the detector supports, the target, and the incident beam.

2.2 Goniometer Construction and Operation

In order to provide a system which was to be easily modified, the goniometer was designed for a modular construction. The mechanical as well as the electrical assemblies are composed of individual, easily removed sections. This design philosophy permits modifications to be easily incorporated into the total system to satisfy the requirements of a specific experiment.

This goniometer is comprised of three basic units joined by one multiconductor cable and by 48-pin connectors. These units are a semi-portable goniometer drive and two control and power supply assemblies, one at the local station and one at the remote. These can be interconnected in either a retracted or an extended configuration allowing for the system to be easily moved from one location to another and to be conveniently tested.

2.2.a Goniometer Drive

The goniometer drive assembly is shown in Figure 2.2. This includes three remotely controlled drive systems which position the target and the 4 foot radius main arm. These systems are rigidly fastened to an adjustable steel and aluminum base (Figure 2.2A). The four threaded steel legs allow the goniometer to be adjusted so that the main arm is located between 3 and 12 inches below the scattering plane. These also permit alignment such that the main arm remains in a level plane during a complete revolution with its center of rotation intersecting the incident beam line. An X-Y stage is also incorporated to allow for a maximum of 1 inch of adjustment in the horizontal plane.

There are two rotating elements in this system which are used to locate detectors with respect to the beam direction (Figure 2.2C). First there is the 4 foot radius, remotely positioned, main arm. This element has a dual beam, counter balanced construction capable of supporting a maximum of 100 lbs at a radius of 4 feet. The dual beam design allows the vertical cryostat, Ge(Li) detector package along with its LN_2 dewar to be securely supported between the minimum and maximum radial positions.

This arm is driven by a Slo-Syn, SS1800-1005, bifilar stepping motor which is operated in both an AC synchronous mode with a speed of 72 RPM and in a DC stepping mode with 200 steps/revolution at a speed of 20

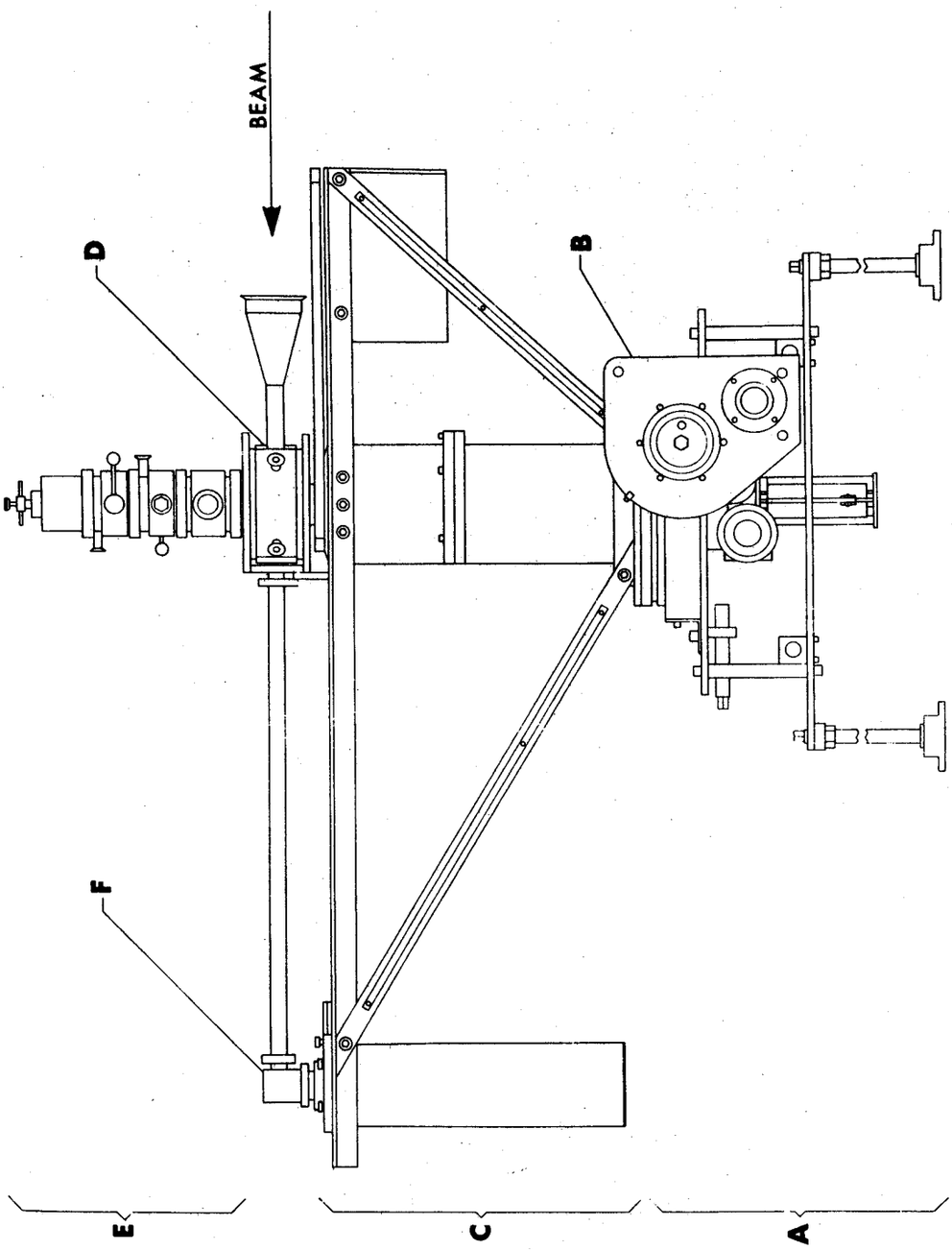

2.2 Goniometer drive unit: A - Base, B - Main arm gear train, C - Main arm, D - Target chamber, E - Target lock, F - Detector carriage.

steps/sec. The motor is connected to the main arm through a 4:1 gear train (see Figure 2.2B) and a 90:1 worm gear. This worm gear mechanism is a Bridgeport, 15 inch, rotary mill table. The resulting rotational velocities of the arm are 72°/min with the motor running in the AC mode and 6°/min for DC operation.

This table is a precision device and precautions were taken to prevent overloading the gears which it contained. To permit the use of the maximum load described above, it was necessary to construct an arm which allowed for a small flex when the angular position of the element was changed. The details of these considerations are given in Appendix I.

The angular position of the main arm is indicated by a vernier scale with a least count of 0.005° and a remote digital readout with a least count of 0.02°. The digital counter is driven by a pair of synchro motors which is connected directly to the Slo-Syn motor shaft.

The second detector positioning element is a 3/4 inch thick aluminum arm located just above the main arm. This manually positioned element has a radius of about 2 feet, and is designed to support maximum loads of about 50 lbs. The angular position is indicated relative to the main arm by a vernier scale with a least count of 0.1°.

The drive mechanisms for the target angle and target height are located below the rotary table. Both of these utilize a worm gear driven by a dual speed motor system.

The position of the target is indicated on two remote digital readouts each of which is driven by a pair of synchro motors which is in turn connected to the drive motor shaft. The least count on the angle readout is 0.02° while the height is 0.2 mil. The gear train used in changing the angular position of the target results in an angular velocity of 432°/min in the fast mode and 36°/min in the slow mode. The target height can be varied at a speed of 1.80 or 0.072 inches/minute. Below the target drive elements are located five microswitches which are activated by a cam on the end of the target shaft. Two of these switches define the target height limits of travel while the remaining define the predetermined positions for three targets in the target holder.

Located just above the arms of the goniometer is the target vacuum chamber (Figure 2.2D), containing a 6 inch high target ladder. The exact configuration of this chamber depends on the experimental needs. These determine, for example, what type of monitor port is incorporated and its position. Also, the experiment dictates the type of beam entrance and exit ports used and the type of coupling needed between the detector and the target vacuum chamber.

The target chamber was designed to be easily modified by providing a replaceable section in the median plane. The first section constructed is 8 inches in diameter and

has two fixed monitor ports at -45° and -135°, a slot for the scattered particles from -15° to 170°, and a single beam port. There is an O-ring seal around the outside of the slot which permits the use of a sliding vacuum seal as well as a thin foil window.

The sliding seal is similar to others (Fe 66) (Bo 67) and was designed to be used with Ge(Li) detectors in a windowless geometry. The seal strap is made of 10 mil stainless steel and is rotated using only the scattered beam port to transfer the torque between the main arm and the strap. The lubrication of this seal which provides a satisfactory operation is Dow Corning, high vacuum, silicone grease. A mixture of vacuum grease and oil with molydenum disulfide powder was also tried but was rejected because it was less convenient to use.

A thin foil window of 1/2 mil Kapton* has also been successfully used in place of the sliding seal on this chamber. Both of these designs are used with an external beam dump located beyond the goniometer. As a result the particle beam must pass through either the foil window or the steel strap. In the latter case serious background radiation is produced and is, therefore, a limitation to the usefulness of this design.

In order to remove this limitation of the 8 inch chamber a 16 inch diameter section was fabricated with the

*E. I. DuPont de Nemours, Wilmington, Delaware.

following features: It includes a sliding seal with a similar construction as the first, and extends from 8° to 110°. This still allows the angular distributions to be obtained, however, from 8° to 172° accomplished by rotating the chamber 180°. It also includes a windowless beam exit port as well as an entrance port, along with two monitor slots with removable thin foil windows of Kapton.

A target transfer and hold lock (Figure 2.2E) is connected to the top of the target chamber through a standard, 4 inch, Marman vacuum coupling. This lock consists of two vacuum valves and a small chamber containing a transfer mechanism. This assembly can be used to insert a target into the central chamber without breaking the chamber vacuum or, if necessary, without exposing the target to the atmosphere.

The detector carriage is shown in Figure 2.2F. The detector packages and the LN_2 dewar are held by this support between the dual beams of the main arm. The radial position of the detector is fixed securely when the detector mount is tightened and the carriage is pinned to the main arm with 1/4 inch, steel dowels. In addition to the single detector mount shown here, a dual mount has been made for holding two detectors side by side. The LN_2 dewar used with this latter system has a pot life of about 10 hours.